Bull. Chem. Soc. Ethiop. **2024**, 38(4), 1163-1175.
DOI: https://dx.doi.org/10.4314/bcse.v38i4.27
© 2024 Chemical Society of Ethiopia and The Authors
ISSN 1011-3924
Printed in Ethiopia
Online ISSN 1726-801X

CORROSION, WEAR AND MACHINABILITY STUDIES ON SCRAP ALUMINIUM ALLOY WHEEL BASED METAL MATRIX COMPOSITE

V.P. Ravi[1*] and R.A. Sankaran[2]

[1]Government Polytechnic College, Palacode, Dharmapuri-636808, India
[2]Salem College of Engineering and Technology, Salem-636111, India

(Received January 4, 2024; Revised February 29, 2024; Accepted March 2, 2024)

ABSTRACT. Recycled materials, especially scrap aluminum alloy wheels with reinforcement castings, are gaining applications in various fields such as aerospace, naval, military, and automobile. In this research, Honda car alloy wheels are stir-cast with 5% alumina as reinforcement and subjected to corrosion, wear, and machinability studies. Corrosion studies were conducted to evaluate the corrosion current density (I_{Corr}), corrosion potential (E_{Corr}), and corrosion rate for the cast aluminum metal matrix composite. The wear studies with different loads, i.e., 50 N, 60 N, 70 N, and 80 N, were performed on the specimen and investigated the coefficient of friction, frictional force, and pin temperature. The sliding load has a significant effect on wear performance, and for the sliding load of 80 N, the wear recorded was 2574.83 µm. The electrochemical machinability studies with voltage, duty cycle, and concentration of citric acid electrolyte are performed on the machining rate and surface corrosion factor. Analysis of the electrochemical machining process with PROMETHEE-II shows that 7 V, 60% duty cycle, and 30 g/L electrolyte concentration are estimated to be the best combination for a higher machining rate and a lower surface corrosion factor.

KEY WORDS: Alumina, Machining rate, Nyquist plot, Electrochemical machining, PROMETHEE-II

INTRODUCTION

The demand for aluminum metal matrix composites (AMMCs) is growing due to their advantages, such as their high strength-to-weight ratio, cost-effectiveness, and good wear strength [1-3]. The extraction of aluminum from ore involves huge effort, such as the utilization of high-heat energy and energy-intensive mining methods. The scrap aluminum alloy wheels (SAAWs) have a notable amount of aluminum that can be recycled, thereby reducing greenhouse gas emissions [4]. Research on the production, testing, and machinability of SAAW-AMMCs has been pursued worldwide. John Victor Chirsty *et al.* [5] have optimized the stir casting process and studied the microstructural properties of SAAW composites. The study revealed that the optimized stir casting variables show low porosity and high compressive strength; moreover, the microstructure shows different patterns in the distribution of reinforcement. Seeniappan *et al.* [6] have optimized the electrochemical machining parameters on SAAW-AMMC. They used grey relational grade to predict the optimal setting as 8 V, 20 g/lit, 50%, and 40 °C for a higher machining rate, a lower overcut, and a lower delamination factor. Kannan *et al.* [7] studied the wear characteristics of hybrid MMC and reported that an increase in sliding load results in a higher coefficient of friction and wear. The reinforcement composition found to have the best wear resistance properties is nano-size alumina at 2% and micro-size alumina at 7% and 5.5%, respectively. Rajmohan *et al.* [8] studied the mechanical and wear properties of the AMMC and reported that good hardness, strength, and wear are attained with Al/10SiC-3mica composites. The increase in mass of mica reduces the wear loss of the composites. Idusuyi and Olayinka [9] have studied the wear properties of metal matrix composites, and their study shows that hardness and an increase in reinforcement particles increase the wear resistance of Al MMCs. Bandil *et al.* [10] studied the micro-structural, corrosion, and mechanical properties of MMC and reported that the aluminum material reinforced

*Corresponding authors. E-mail: ravikavithagpt@gmail.com
This work is licensed under the Creative Commons Attribution 4.0 International License

with 20% reinforcement demonstrated the minimum corrosion. The tribological and corrosion performances fully depend on the reinforcement percentage. Kumar *et al.* [11] have studied the corrosion properties of aluminum alloys reinforced with zirconium di-boride. The aluminum alloy with reinforcement (AA7178-ZrB_2) shows superior corrosion resistance than the aluminum alloy (AA7178). The metal matrix composites developed were subjected to machinability studies, especially through unconventional machining methods since the machining of metal matrix composites is complex through conventional machining [12-15]. As per the literature, it is evident that research on AMMCs has been pursued by the researchers and archived in the database about the performance of reinforcement percentage, type of reinforcement, size of reinforcement on wear, structural, mechanical, and corrosion properties. In addition to this, the research studies on SAAW-based AMMC are sparse, especially on corrosion, wear, and machinability studies. Hence, in this research, SAAW-based AMMC was fabricated through the stir casting process, and corrosion, wear, and machinability were performed to understand the performance of the fabricated SAAW-AMMC.

EXPERIMENTAL

Casting of sample

The sample is cast using a stir-casting furnace with a bottom pouring type. This furnace is an automated casting machine with advanced features, and the process parameters are controlled using a hand-held Android device with a wireless interface. The car wheel of a Honda was obtained from the scrap vendor, and the elements present in wt.% are Al (83.62), Si (3.81), Fe (2.92), Sn (0.19), Zn (0.06), Cu (0.09), Ti (0.17), Mn (1.62), and Mg (2.74) [14]. The process parameters setting for casting are: stirrer temperature is maintained at 750 °C, speed of stirrer is maintained at 650 rpm, time of stirring is 10 min, and squeeze pressure is 200 MPa [16]. Figure 1 shows the EDAX analysis of the SAAW-MMC specimen with peaks of silica, aluminum, nickel, manganese, and iron.

Potentiodynamic polarization test (PDP)

The electrochemical performance of the sample was assessed with the help of a potentiodynamic polarization test by means of a potentiostat. The cast samples were cut into 50 × 50 × 30 mm pieces and mechanically polished with 2000-grit SiC paper. The sample is fixed to the holder prior to being kept in a flask consisting of a 3.5 wt% sodium chloride solution at room temperature [17]. The electrochemical cell consists of an operating electrode, a reference electrode, and a counter electrode made up of casted MMC, saturated calomel, and platinum, respectively. The corrosion potential scanning range was kept between −600 and 1.6 mV, with a 1 mV/s scanning speed. The corrosion frequency, ability of corrosion, and current intensity of the samples were evaluated with the Tafel extrapolation technique. Corrosion current density is the measure of a metal's rate of deterioration in a particular environment.

Wear test

As per ASTM G99, a sample of SAAW AMMCs was prepared with a diameter of 10 mm and a height of 30 mm [7]. Prior to loading the sample into the wear test rig, the surface of the sample is prepared by polishing it using fine disc sandpaper (320 grit) and thoroughly cleaning it with alcohol. An EN31 disc material with a hardness of 63 HRC was used, and Table 1 provides the wear testing parameters, including material specifications. The composites after the wear tests were analyzed using a scanning electron microscope (FESEM) of Shimadzu make and model: UV-1700 with Energy Dispersive Spectroscopy (EDS).

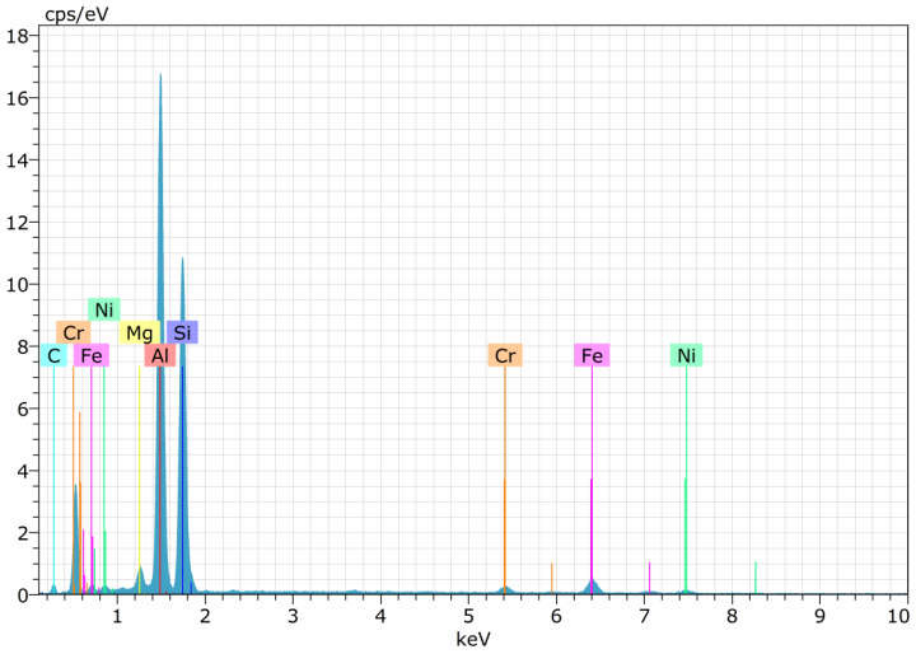

Figure 1. EDAX of SAAW- MMC.

Table 1. Wear studies parameters.

Parameters	Description
Wear test standard	ASTM-G99
Pin material	AMMC (SAAW with 5% alumina) Size: diameter: 10 mm, length: 30 mm
Disc material	Hard bearing steel EN31 Size: Dia: 100, Thickness: 8 mm; Initial roughness, Ra: 0.20–0.25 µm
Load applied	50, 60,70 & 80 N
Sliding velocity	0.785m/s
Test Duration	900 s
Sliding distance	707mm
Sliding condition	Dry

Electrochemical machining (ECM) setup

The ECM setup used for machining consists of four subsystems: machine structure, tool electrode advancing system with controller, electrolyte circulation system, and power supply unit. The machine structure houses the machining chamber in which the workpiece is fixed to the fixture. The electrolyte supply system consists of a pump and filtering system. The tool feeding system consists of a stepper motor and a microcontroller unit. The movement of the tool electrode is controlled by this unit. The pulsed power supply unit provides the power supply to the anode (workpiece) and cathode (tool electrode). The citric electrolyte is used for the experiments, and the parameters, namely voltage, electrolyte concentration, and duty cycle, are varied depending on the machining speed and corrosion factor. The machining speed is evaluated based on the

machining time to complete and the thickness of the workpiece. The surface corrosion factor is determined by finding the length ratio between the hole diameter and pitting area. The L9 orthogonal array (OA) experiments depicted in Table 2 are considered based on the calculated degrees of freedom. Totally, 3 factors are considered at 3 levels; hence, the degrees of freedom are calculated as 6, i.e., 3(3-1). Hence, the OA selected should be greater than the degrees of freedom; therefore, L9 OA is selected. The ECM setup comprises the tool forwarding mechanism, power supply unit, and electrolyte circulating system [18]. The sample SAAW-AMMC of 50 × 50 × 3 mm is used as a workpiece, and a tool electrode of diameter 380 µm was coated with bonding resin to prevent stray current. The citric electrolyte is prepared by mixing the different grams of citric salt in one liter of distilled water.

Table 2. L_9 OA experiment scheme.

Expt. No.	Voltage in volts	Duty cycle in %	Electrolyte concentration in g/L	Machining rate in µm/s	Surface corrosion factor
1	6	60	20	0.253	1.851
2	6	70	30	0.287	1.758
3	6	80	40	0.422	2.112
4	7	60	30	0.275	2.307
5	7	70	40	0.351	2
6	7	80	20	0.333	2.166
7	8	60	40	0.301	2.031
8	8	70	20	0.316	2.017
9	8	80	30	0.395	2.289

The preference ranking organization method of enrichment evaluation (PROMETHEE II) method

PROMETHEE-II is the prominent method considered for the multi-criteria problems, which outranks the performance characteristics of the favorability function method. The PROMETHEE II method simplifies the computational procedure and lessens the number of comparisons [4, 19]. In this method, the ideal criteria function, equivalent process variables, and favorite function F_α (i, j) devolve on the pairwise dissimilarity P_α among the estimates I_α(i) and I_α(j) of the options a and b for the criterion α.

Table 3 shows two types of criterion functions. The component Dα is the highest level of indifference and designates the largest difference, which is insignificant when measuring up the two alternatives in relation to that criterion. The weights for each factor are 0.5.

Multi-criteria preference index (i, j), a weighted average function P_α(i, j) for every criterion, is denoted as [4, 18]:

$$£(i,j) = \frac{\sum_{\alpha=1}^{\beta} X_\alpha F_\alpha(i,j)}{\sum_{\alpha=1}^{n} w_\alpha} \quad (1)$$

$$\rho^+(i) = \frac{\sum_A \varepsilon(i,j)}{P-1} \quad (2)$$

$$\rho^-(i) = \frac{\sum_A \varepsilon(i,j)}{S-1} \quad (3)$$

$$\rho(i) = \rho^+(i) - \rho^-(i) \quad (4)$$

where X_α = weight of the criterion α; (i) = indicator in the alternatives set S; β = no. of criteria. The best or most appropriate experiment is the one with the highest ρ value.

Table 3. Functions for criteria and appropriate preference values [4].

S. No.	Criterion functions	Values of choice
1	Normal criterion	$G(D_\alpha) = \begin{bmatrix} 0 & if & D_\alpha = 0 \\ 1 & if & D_\alpha > 0 \end{bmatrix}$
2	Quasi criterion	$G(D_\alpha) = \begin{bmatrix} 0 & if & D_\alpha \leq d_\alpha \\ 1 & if & Ds_\alpha > d_\alpha \end{bmatrix}$

Steps of PROMETHEE-2 methodology

(1) Using the basic data, an evaluation matrix that reports each alternative's performance in relation to each criterion must be constructed. (2) To ascertain the variations in performance (Dα) for every pair of alternatives about every criterion. (3) Select the criteria function type, as well as the threshold values for indifference and first choice for each criterion. (4) The combined preference indices for every pair of options are calculated. (5) Finding the outranking flows. (6) Choosing the optimal option with the highest outranking value ρ(i).

RESULTS AND DISCUSSION

Potentiodynamic polarization test (PDP)

The corrosion current density (I_{corr}) and corrosion potential (E_{corr}) were calculated from the intersection of the tangent constructed for cathodic and anodic Tafel curves, presented in Figure 2. Figure 2 shows the graph of the potentiodynamic polarization curve of SAAW MMC. Based on the literature, the I_{corr} (mA/cm^2) for aluminum alloy is found to be 31.623, and with the reinforcement of fly ash, it shows 3.162 V [20]. In the same way, the corrosion current density of SAAW MMC is found to be 14.476 µA, it is evident that the inclusion of 5% alumina lowers the corrosion current density. The I_{corr} of the sample was used to determine the material's resistance to corrosion. In the case of the corrosion potential (E_{corr}) of the aluminum alloy, it is found to be -5.8 V in the literature, and the E_{corr} obtained from the SAAW MMC is greater than that of the aluminum alloy. This means that adding alumina micro-particles improved their corrosion ability, having the greatest E_{corr} (-0.260307 V). The increase in the corrosion rate of SAAW MMC was associated with the dispersion of alumina particles. The corrosion rate is found to be 6.2104 mpy.

The resistance of the electron transfer process in relation to electrode surfaces is determined by the curves in Nyquist plots, as shown in Figure 3. EIS data were plotted on a Nyquist plot, shown in Figure 3, and analyzed by fitting them into an equivalent circuit, shown in Figure 3. The circuit consists of the ohmic resistance of the electrolyte, the capacitance of the surface layer, and the resistance of the surface layer. The capacitance of the surface layer is an ideal capacitor, which could not be used due to the roughness of the layer. The values of the ohmic resistance of the electrolyte are similar to the resistance attributed to the electrolyte. On the other hand, the resistance of the surface layer increases with the reduction of pores and voids. The addition of 5% alumina results in insulation of the metal and solution interface, resulting in enhanced charge transfer resistance and higher corrosion resistance.

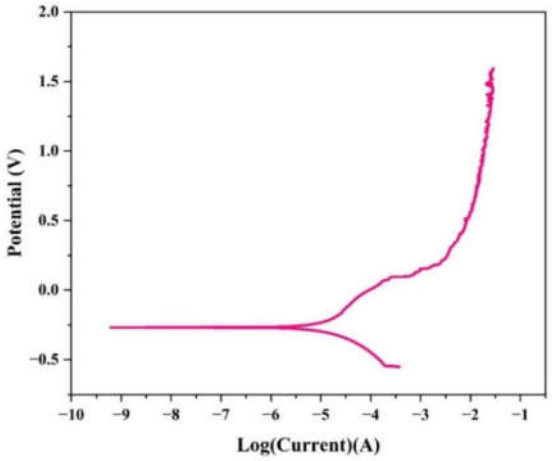

Figure 2. Potentiodynamic polarization curves.

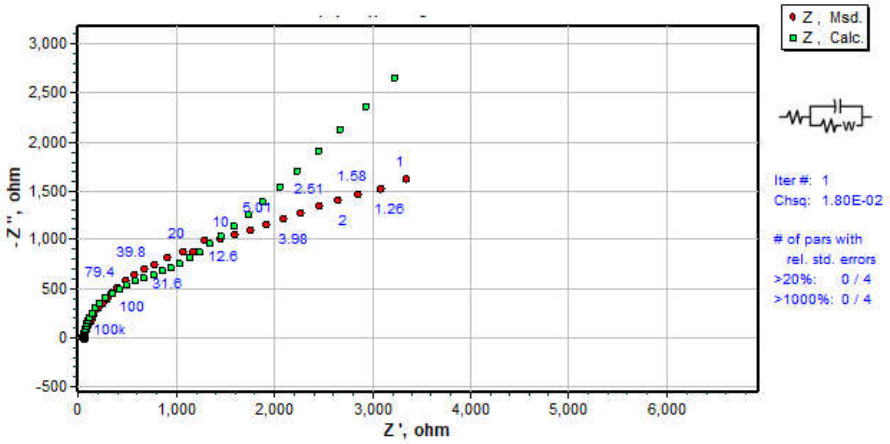

Figure 3. Nyquist plot of the SAAW- MMC.

Wear analysis

When the surfaces of two objects come into contact, friction is the force that prevents motion. Figure 4(a-d) depicts the coefficient of friction, frictional force, pin temperature, and wear at a load of 50 N. It is clear from the figures that the coefficient of friction is found to vary between 0.001 and 0.003, and the frictional force is found to be 0.156 N. The wear graph gradually increases and reaches its maximum value at 252.78 µm, and throughout the process, the pin temperature varies between 33 °C and 40 °C. With an increase in load to 60 N, the maximum frictional force and coefficient of friction reduce to 0.127 N and 0.002, respectively, as depicted in Figure 4(e-h). In Figure 4(i-l), the maximum wear is noticed at 191.758 µm, and the pin

temperature of the wear varies between 38 °C and 42.5 °C. With the increase in load to 70 N, the frictional force is recorded as 0.264 N, which is comparatively high, and the coefficient of friction is recorded as 0. 0032. The quantity of material removed per unit of time is known as the wear rate. It is the material's most important characteristic for comprehending its function and longevity in mechanical components. The wear noticed is 136.24 µm, and the temperature of the pin varies between 39 °C and 43 °C. Figure 4(m-p) shows the highest wear of 2574.83 µ, and pin temperature varies between 40 °C and 44.22 °C. It is evident from the above observation that an increase in sliding load has a significant effect on the wear of the material. The modification of the sliding load augments the deformation and fracturing of the soft surface of the SAAW-MMC, resulting in more wear. Figures 5 (a and b) shows the shallow and hard wear marks on the surface of the SAAW-MMC. When loads are low, worn surfaces of composite specimens normally have shallow wear marks, and at high loads, severe wear marks are noticed on the surfaces.

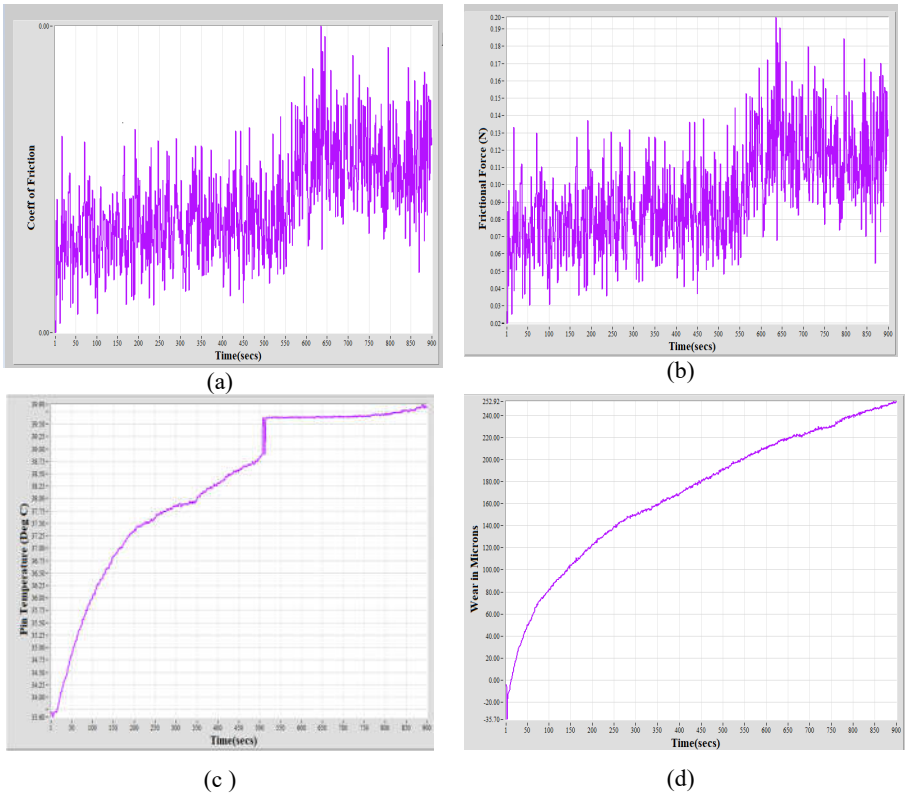

Figure 4(a-d). Coefficient of friction, frictional force, pin temperature and wear at 50 N.

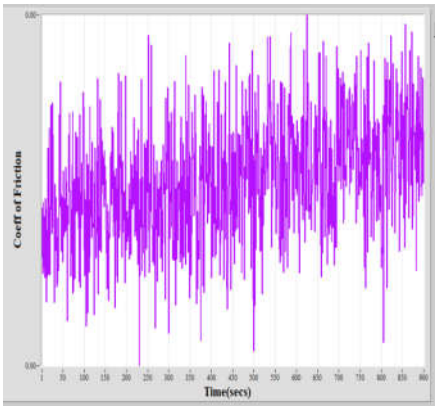

(e)

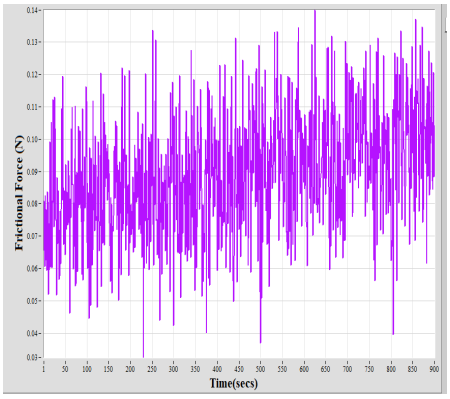

(f)

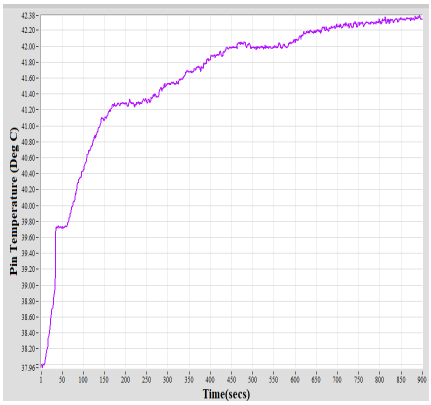

(g)

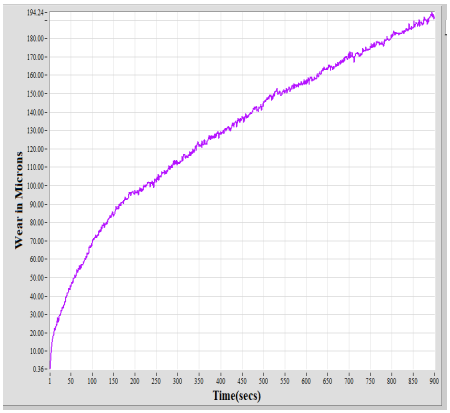

(h)

Figure 4(e-h). Coefficient of friction, frictional force, pin temperature and wear at 60 N.

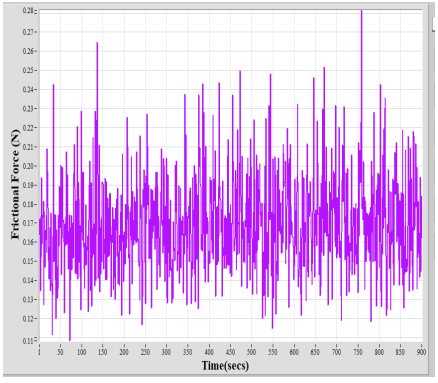

(i)

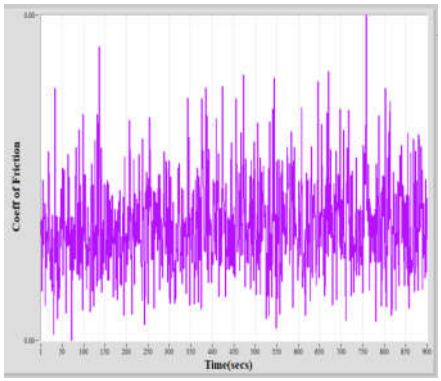

(j)

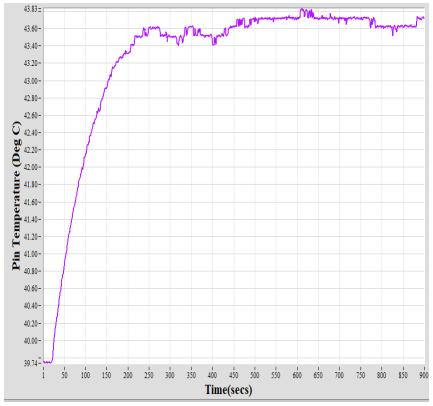

(k)

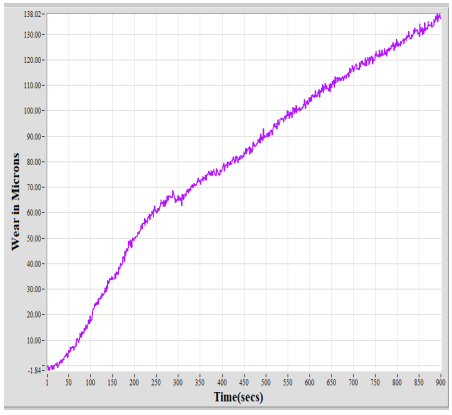

(l)

Figure 4(i-l). Coefficient of friction, frictional force, pin temperature and wear at 70 N.

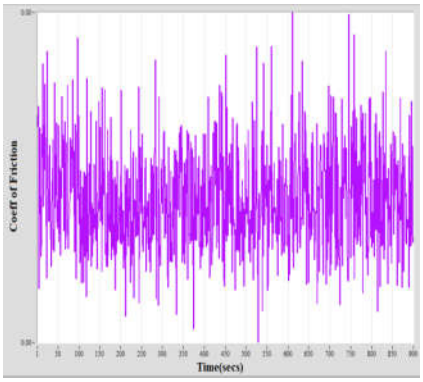

(m)

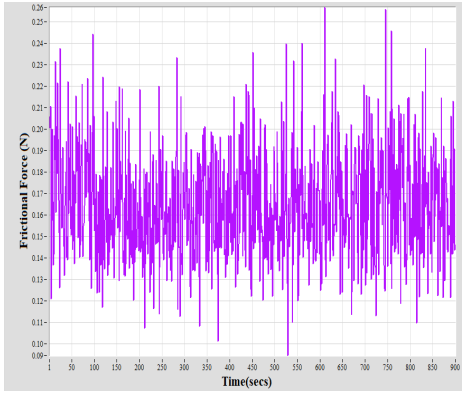

(n)

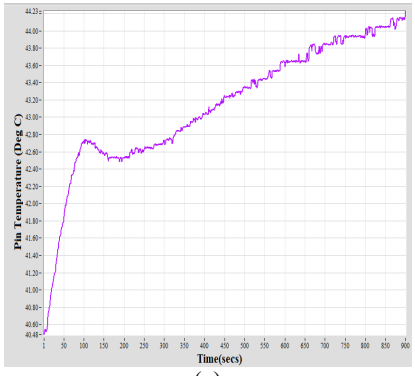

(o)

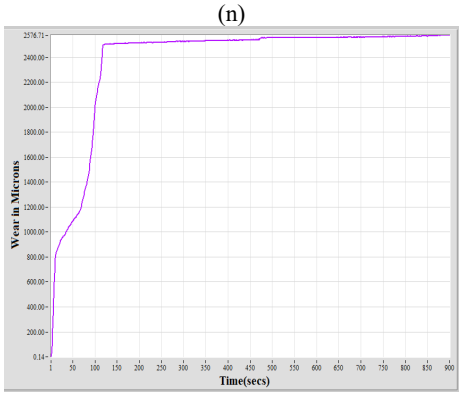

(p)

Figure 4(m-p). Coefficient of friction, frictional force, pin temperature and wear at 80 N.

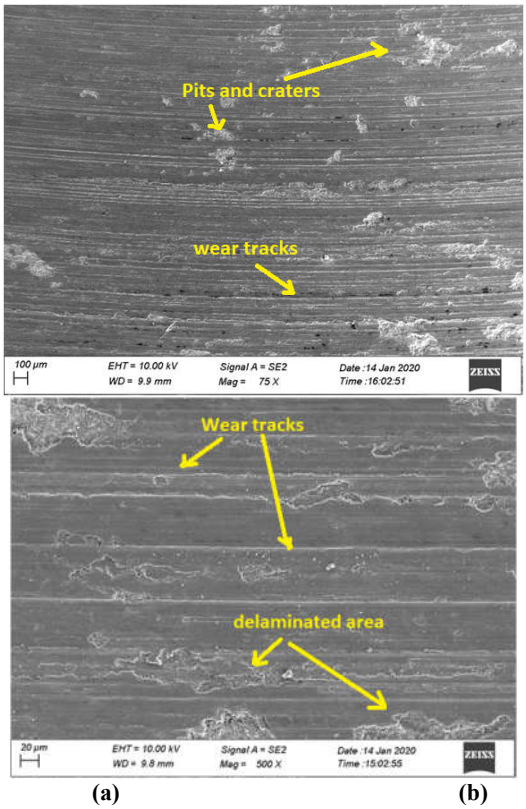

Figures 5. SEM pictures of surface with (a) wear tracks and (b) delaminated area.

Analysis of PROMETHEE-II

Using equations 1–4, the transformed payoff matrix is given in Table 4. The pair-wise dissimilarity of all values of alternatives for every nine criteria in Table 4 was estimated. The weight for each criterion is given as 0.3333 and estimated, and ρ as per equations 2-4 and presented in Table 4.

As per the analysis, 7 V, 60% duty cycle, and 30 g/L electrolyte concentration are estimated as the best combination for a higher machining rate and a lower surface corrosion factor, and the next best combination is 8 V, 80% duty cycle, and 30 g/L. While analyzing the SEM micrograph (Figure 6), more pitting is observed on the circumference of the machined hole. In spite of the electrode insulation, the stray current-affected zone is witnessed in the machined area [20]. The electrochemical erosion removes the reinforcement along with the matrix material, resulting in macro-pits. Figure 6 depicts the micro-hole with a circular profile, and little debris is noticed due to improper flushing. Although delaminated regions are prevalent in the MMC during machining, a few regions in the hole expose the delaminated surface, as depicted here, which was machined at optimal machine settings.

Table 4. Transformed payoff matrix and ranking pattern for alternatives.

Machining rate µm/sec	Surface corrosion factor	$\rho^+(i)$	$\rho^-(i)$	$\rho(i)$	Rank
0.253	-1.851	0.500	0.389	0.111	-
0.287	-1.758	0.333	0.556	-0.222	-
0.422	-2.112	0.278	0.643	-0.365	-
0.275	-2.307	0.833	0.000	0.833	1
0.351	-2	0.222	0.700	-0.478	
0.333	-2.166	0.500	0.375	0.125	
0.301	-2.031	0.500	0.167	0.333	3
0.316	-2.017	0.389	0.250	0.139	-
0.395	-2.289	0.444	0.000	0.444	2

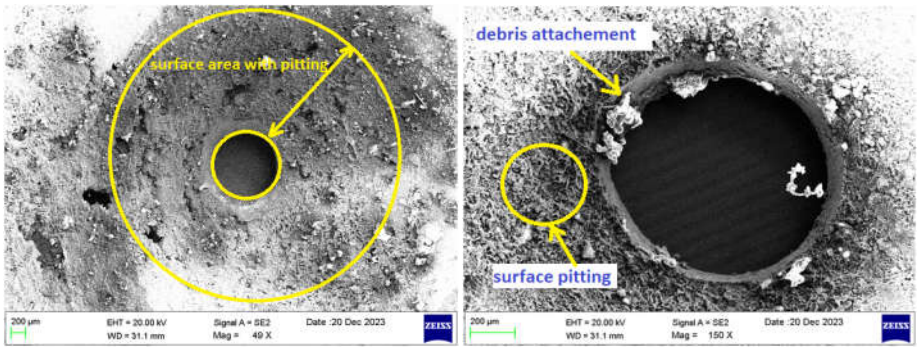

(a) (b)

Figure 6. Microhole (a) with surface pitting and (b) machined at optimal setting.

CONCLUSION

The SAAW MMC with 5% alumina was successfully cast using the stir casting setup. The casted bar is cut into suitable dimensions, and various studies such as corrosion performance, wear characteristics, and machinability studies using ECM were performed. The corrosion property investigation reveals that the corrosion current density (I_{Corr}), corrosion potential (E_{Corr}), and corrosion rate of the casted SAAW MMC were 14.476 µA, -0.260307 V, and 6.2104 mpy. The wear study reveals that with the increase in load to 70 N, the frictional force was recorded at 0.264 N, which is comparatively high, and the coefficient of friction was recorded at 0.0032. The sliding load has a significant effect on wear performance, and for the sliding load of 80 N, the wear recorded was 2574.83 µm. Electrochemical machinability studies were conducted with the L_9 OA plan, and the parameter levels were optimized using PROMETHEE-II on machining rate and surface corrosion factor. Analysis of the electrochemical machining process shows that 7 V, 60% duty cycle, and 30 g/L electrolyte concentration are estimated to be the best combination for a higher machining rate and a lower surface corrosion factor. The studies can be extended by analyzing the use of sea water as an electrolyte on the SAAW MMC in the ECM. Moreover, different compositions of SAAW MMC can be prepared, and comparative corrosion studies can be conducted.

REFERENCES

1. Mourad, A.H.I.; Christy, J.V.; Krishnan, P.K.; Mozumder, M.S. Production of novel recycled hybrid metal matrix composites using optimized stir squeeze casting technique. *J. Manuf. Process.* **2023**, 88, 45-58.
2. Maniraj, S.; Thanigaivelan, R.; Viswanathan, R.; Elumalai, P. Experimental investigation of MRR and ROC in aluminium metal matrix composites. *Mater. Today: Proceed.* **2021**, 45, 1102-1106.
3. Kumar, G.P.; Thanigaivelan, R.; Arunachalam, R.M.; Paramasivam, P. Experimental investigation of EDM processing parameters on machining Al_6O_{63}-12% SiC-5% Gr using response surface methodology. *High Temp. Mater. Process.* **2014**, 18, 27-43.
4. Annamalai, P.; Dhavamani, C. Experimental investigation on machining of recycled aluminum alloy metal matrix composite in ECMM. *Trans. Indian. Inst. Met.* **2023**, 76, 1831-1839.
5. Christy, J. V.; Arunachalam, R.; Mourad, A. H. I.; Krishnan, P. K.; Piya, S.; Al-Maharbi, M. (2020). Processing, properties, and microstructure of recycled aluminum alloy composites produced through an optimized stir and squeeze casting processes. *J. Manuf. Process.* **2020**, *59*, 287-301.
6. Seeniappan, K.; Patil, P.; Ganesan, S.K.; Thanigaivelan, R. Development and performance optimization of ECM parameters on scrapped alloy wheel metal matrix composites. *High Temp. Mater. Processes*. **2024**, 28, 2, 33-43
7. Kannan, P.R.; Thanigaivelan, R.; Thiraviam, R.; Kumar, K.P. Performance studies on hybrid nano-metal matrix composites for wear and surface quality. *Mater. Sci.-Pol.* **2023**, 41, 288-300.
8. Rajmohan, T.; Palanikumar, K.; Ranganathan, S. Evaluation of mechanical and wear properties of hybrid aluminium matrix composites. *Trans Nonferrous Met. Soc. China* **2013**, 23, 2509-2517.
9. Idusuyi, N.; Olayinka, J.I. Dry sliding wear characteristics of aluminium metal matrix composites: a brief overview. *J. Mater. Res. Technol.* **2019**, 8, 3338-3346.
10. Bandil, K.; Vashisth, H.; Kumar, S.; Verma, L.; Jamwal, A.; Kumar, D.; Gupta, P. Microstructural, mechanical and corrosion behaviour of Al–Si alloy reinforced with SiC metal matrix composite. *J. Compos. Mater*. **2019**, 53, 4215-4223.
11. Kumar, S.D.; Ravichandran, M.; Jeevika, A.; Stalin, B.; Kailasanathan, C.; Karthick, A. Effect of ZrB_2 on microstructural, mechanical and corrosion behaviour of aluminium (AA7178) alloy matrix composite prepared by the stir casting route. *Ceram. Int.* **2021**, 47, 12951-12962.
12. Rajan, N.; Sri, M.N.; Anusha, P.; Thanigaivelan, R.; Vijayakumar, S. Performance optimization of electrochemical machining parameters on aluminum metal matrix composite. *Surf. Eng. Appl. Electrochem*. **2023**, 59, 719-727.
13. Sharma, S.; Sudhakara, P. Fabrication and optimization of hybrid AA-6082-T6 alloy/8% Al_2O_3 (alumina)/2% Grp metal matrix composites using novel Box-Behnken methodology processed by wire-sinking electric discharge machining. *Mater. Res. Express.* **2019**, 6, 116594.
14. Palaniswamy, V.; Rajasekaran, T. Performance of magnetized tool in electrochemical micromachining on scrapped alloy wheel matrix composite. *J. Electrochem. Sci. Eng*. **2023**, 13, 553-561.
15. Zhou, B.; Liu, B.; Zhang, S.; Lin, R.; Jiang, Y., Lan, X. Microstructure evolution of recycled 7075 aluminum alloy and its mechanical and corrosion properties. *J. Alloys Compd.* **2021**, 879, 160407.
16. Krishnan, P.K.; Christy, J.V.; Arunachalam, R.; Mourad, A.H.I.; Muraliraja, R.; Al-Maharbi, M.; Chandra, M.M. Production of aluminum alloy-based metal matrix composites using scrap

aluminum alloy and waste materials: Influence on microstructure and mechanical properties. *J. Alloys Compd.* **2019**, 784, 1047-1061.
17. Krishnan, P.; Lakshmanan, P.; Annamalai, G. Impact of nano-SiC_P and nano-hBN_P on the corrosion performance and fatigue behavior of Mg–Zn hybrid nanocomposites, *Corros. Mater.* **2023**, 74, 403-418.
18. Thanigaivelan, R.; Senthilkumar, R.; Arunachalam, R.M.; Natarajan, N. Impact of the shape of electrode-tool on radical overcut of micro-hole in electrochemical micromachining. *Surf. Engin. Appl. Electrochem.* **2017**, 53, 486-492.
19. Deepa, D.; Thanigaivelan, R.; Gunasekaran, K.; Praveenkumar, S. A comparative study of natural convective transfer in rectangular and square geometry micro fins. *Tecnica Italiana-Italian J. Eng. Sci.* **2021**, 65, 446-449.
20. Sivashanka, N.; Thanigaivelan, R.; Saravanan, K.G. Electrochemical micromachining and parameter optimization on AZ31 alloy—ANN and TOPSIS techniques, *Bull. Chem. Soc. Ethiop.* **2023**, 37, 1263-1273.